Editors' Suggestion

Electrically tunable high-Chern-number quasiflat bands in twisted antiferromagnetic topological insulators

Huaiqiang Wang,[1] Yiliang Fan,[2] and Haijun Zhang[2,3,*]

[1]*Center for Quantum Transport and Thermal Energy Science, School of Physics and Technology, Nanjing Normal University, Nanjing 210023, China*

[2]*National Laboratory of Solid State Microstructures, School of Physics, Nanjing University, Nanjing 210093, China*

[3]*Collaborative Innovation Center of Advanced Microstructures, Nanjing University, Nanjing 210093, China*

(Received 8 April 2024; revised 2 July 2024; accepted 29 July 2024; published 14 August 2024)

Isolated flat bands with significantly quenched kinetic energy of electrons could give rise to exotic strongly correlated states from electron-electron interactions. More intriguingly, the interplay between topology and flat bands can further lead to richer physical phenomena, which have attracted much interest. Here, taking advantage of the recently proposed intertwined Dirac states induced from the anisotropic coupling between the top and bottom surface states of an antiferromagnetic topological insulator thin film, we show the emergence of a high-Chern-number (quasi)flat-band state through moiré engineering of the surface states. Remarkably, the flat bands are isolated from other bands and located near the Fermi level. Furthermore, topological phase transitions between trivial and nontrivial flat-band states can be driven by tuning the out-of-plane electric field. Our work not only proposes a scheme to realize high-Chern-number flat-band states, but also highlights the versatility of the intertwined Dirac-cone states.

DOI: 10.1103/PhysRevB.110.085135

I. INTRODUCTION

Recently, the seminal experimental findings of unconventional superconductivity and correlated insulator behavior in twisted bilayer graphene (TBG) [1,2] have ignited a surge of research interest in condensed-matter systems hosting flat-band electronic structures. In these flat bands, the kinetic energy of electrons is significantly quenched, and electron-electron interactions become dominant, which could give birth to exotic strongly correlated states, such as the fractional quantum Hall effect (FQHE) [3], fractional Chern insulators, and fractional topological insulators (TIs) [4–11]. Interestingly, it has been shown that flat bands possessing a high Chern number ($C > 1$) could generate many new states [12–15] beyond the Landau-level-like case with $C = 1$ in the FQHE. This renders realistic platforms possessing isolated high-Chern-number flat bands very attractive and highly desired [16].

As for the realization of flat-band states, moiré engineering of two-dimensional van der Waals heterostructures, e.g., TBG [17,18] and twisted transition metal dichalcogenide multilayers [19–22], has proved to be a versatile tool, where the twist angle plays a very crucial role. Moreover, moiré engineering has also been applied to other Dirac materials, in particular the Dirac-cone surface state (DSS) of three-dimensional TIs [23–25]. However, since the DSS in TIs is anomalous and protected by time-reversal symmetry, it remains gapless and cannot be disconnected from other bands under the moiré superlattice potential. To circumvent this issue, a natural way is to gap the DSS by magnetism, from which isolated moiré flat bands could be obtained [26,27]. To this end, the recently discovered intrinsic magnetic TI $MnBi_2Te_4$ and its family materials [28–56] could serve as promising platforms. Intriguingly, when the TI film becomes very thin, the coupling between the top and bottom DSSs cannot be neglected and usually turns out to be critical in the low-energy physics [57–60]. It is worth mentioning that a recent work [61] by some of the authors proposes that anisotropic couplings between the DSSs of an antiferromagnetic (AFM) TI thin film could give rise to emergent new Dirac cones, dubbed *intertwined Dirac-cone states*, away from the Γ point. It is thus straightforward to expect that the interplay between magnetism, DSS coupling, and moiré engineering can lead to rich new phenomena.

In this paper, based on the effective model analysis, we show the emergence of high-Chern-number ($C = n$) flat-band states through moiré engineering of the two DSSs of an AFM TI film respecting the n-fold ($n = 2, 3, 4, 6$) rotational symmetry in the presence of an out-of-plane electric field. The intertwined Dirac-cone states induced from anisotropic couplings are found to play a significant role in this process. Furthermore, the flat bands are electrically tunable, and taking the $n = 3$ case as an example, we explicitly demonstrate the topological phase transition between trivial ($C = 0$) and nontrivial ($C = 3$) flat-band states. Our work not only proposes a route to obtain high-Chern-number flat bands, but also highlights potential applications of the intertwined Dirac-cone states.

II. MODEL DESCRIPTION

We consider a thin film of AFM TI with opposite out-of-plane (z-axis) magnetic moments on its top and bottom

*Contact author: zhanghj@nju.edu.cn

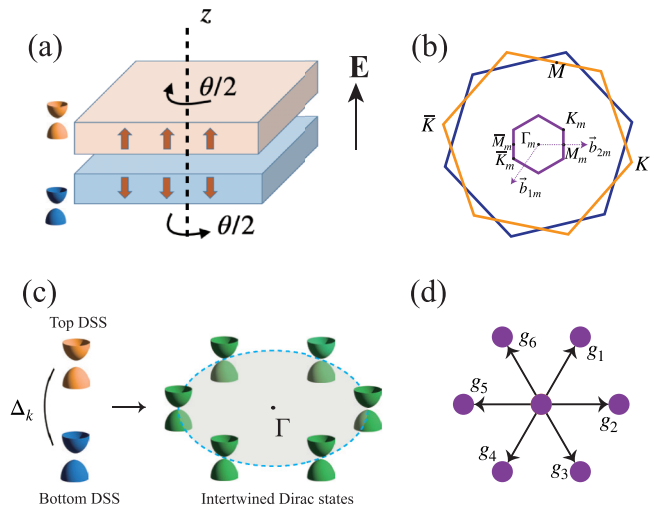

FIG. 1. (a) Schematic of the twisted antiferromagnetic topological insulator thin film under an out-of-plane electric field, where a clockwise (counterclockwise) rotation with angle $\theta/2$ is implemented for the top (bottom) surface layer. (b) Two-dimensional Brillouin zones (BZs) of the top (orange lines) and bottom (blue lines) surface layers after the twist, and the moiré reciprocal vectors (purple dashed lines) and corresponding moiré BZ (purple solid lines). (c) Illustration of the emergent intertwined Dirac-cone states from the coupling between the top and bottom Dirac surface states (DSSs). (d) The first-shell approximation taken in the moiré reciprocal lattices for calculating the interlayer moiré hopping, where the g_i's are the six smallest moiré reciprocal vectors.

surfaces, e.g., an even-layer $MnBi_2Te_4$ film with A-type AFM order, as schematically shown in Fig. 1(a). Apart from the combined $\mathcal{PT}$ symmetry from inversion $\mathcal{P}$ and time-reversal operation $\mathcal{T}$, the AFM TI film is assumed to preserve an additional n-fold ($n = 2, 3, 4, 6$) crystalline rotation symmetry (C_{nz}) along the z direction and a combined symmetry $\mathcal{M}_x\mathcal{T}$ from mirror ($\mathcal{M}_x$) and time-reversal ($\mathcal{T}$) operations. When an electric field E is applied along the out-of-plane direction, the precedent $\mathcal{PT}$ symmetry of the AFM TI film is broken. Further, we implement a clockwise (counterclockwise) rotation of angle $\theta/2$ for the top (bottom) surface layer, leading to a relative twisting angle of θ between them.

To lay a foundation for later discussion, we start from the untwisted case with $\theta = 0$, where the low-energy physics of the AFM TI film can be captured by the top and bottom DSSs and the coupling between them. In the ordered basis of $|t,\uparrow\rangle$, $|t,\downarrow\rangle$, $|b,\uparrow\rangle$, $|b,\downarrow\rangle$, where $t(b)$ represents the top (bottom) DSS, the Hamiltonian can be described as

$$H = \begin{bmatrix} h_t + U\sigma_0 & h_{\text{coup}} \\ h_{\text{coup}}^\dagger & h_b - U\sigma_0 \end{bmatrix}, \tag{1}$$

with

$$h_{t(b)} = \pm\left[v(k_x\sigma_y - k_y\sigma_x) + m\sigma_z + \frac{R_w}{2}(k_+^n + k_-^n)\sigma_z\right],$$
$$h_{\text{coup}} = (\Delta - Bk^2)\sigma_0 - \frac{R_a}{2}(k_+^n - k_-^n)\sigma_0. \tag{2}$$

Here, $k = (k_x^2 + k_y^2)^{1/2}$ and $k_\pm \equiv k_x \pm ik_y$. σ_i's ($i = x, y, z$) are Pauli matrices acting in the spin subspace, and σ_0 is a 2×2 identity matrix. U is the effective staggered potential caused by the electric field between the top and bottom DSSs. The first term in $h_{t(b)}$ describes the helical DSS, with v denoting the Fermi velocity. The $m\sigma_z$ term represents the Zeeman coupling between the DSS and its surrounding magnetic moment, where the coupling strength $|m|$ is simply assumed to be the same for the two DSSs but with opposite signs due to the opposite surface magnetic moments in the AFM TI. The R_w term in $h_{t(b)}$ comes from the warping effect imposed by the rotation symmetry C_{nz} [62,63]. As for the coupling term h_{coup}, it should be emphasized that besides the isotropic coupling up to k^2 order [57–60,64,65], we have taken into account a symmetry-allowed anisotropic coupling, namely, the R_a term. Remarkably, we have shown that the introduction of the anisotropic R_a term can give birth to $2n$ Dirac-cone states located away from the Γ point, as schematically shown in Fig. 1(c). These Dirac cones are termed intertwined Dirac cones, since they are induced from the hybridization of top and bottom DSSs. Furthermore, based on the intertwined Dirac-cone states, a high-Chern-number phase with $C = n$ can be achieved by tuning the potential U [61], which paves the way for designing high-Chern flat bands by twisting the AFM TI thin film as we show below.

Considering the fact that the most well-studied (magnetic) TIs up to now are Bi_2Te_3 and $MnBi_2Te_4$ family materials respecting the threefold rotational symmetry C_{3z}, henceforth we choose the $n = 3$ case in our paper, and the main results should remain valid for other cases of n. Correspondingly, the parameters in our effective model calculations of our paper are chosen in the same order of magnitude as those used in Bi_2Te_3 and $MnBi_2Te_4$ family materials [58,62,63,66]. Figure 1(b) schematically shows the twisted Brillouin zones (BZs) of the top (orange lines) and bottom (blue lines) surface layers, and the moiré BZ (purple lines), where high-symmetry points are explicitly labeled. The moiré reciprocal vectors $\vec{b}_{im}$ ($i = 1, 2$) are given by the difference between the rotated reciprocal vectors of the bottom and top surfaces as $\vec{b}_{im} = \vec{b}_{i,t} - \vec{b}_{i,b}$. The length of $\vec{b}_{im}$ can be obtained as $|\vec{b}_{im}| = 8\pi \sin(\theta/2)/(\sqrt{3}a_0)$, where a_0 is the lattice constant of the surface layer. The Hamiltonian after the twist can be written as

$$H_\theta = \begin{bmatrix} h_{t,-\theta/2} + U\sigma_0 & T \\ T^\dagger & h_{b,\theta/2} - U\sigma_0 \end{bmatrix}, \tag{3}$$

where $h_{t(b),\mp\theta/2} = R_{\mp\theta/2}^\dagger h_{t(b)} R_{\mp\theta/2}$, with $R_{\mp\theta/2} = e^{\pm i\theta\sigma_z/4}$. T represents the spatially periodic intersurface moiré hopping potential, and it suffices [43] to Fourier expand it to the lowest order as

$$T = T_0 + \sum_{j=1}^{6} T_j e^{i\vec{g}_j\cdot\vec{r}}. \tag{4}$$

Here, g_j's are the six smallest moiré reciprocal vectors which can be generated from $\vec{b}_{1m}$ by sixfold rotations, as shown in Fig. 1(d). In the moiré reciprocal lattice, the above approximation amounts to considering the couplings within the first-shell reciprocal lattices spanned by g_j's.

III. HIGH-CHERN-NUMBER QUASIFLAT BANDS

For later reference, we first briefly review the emergence of high-Chern-number state in the untwisted case, the details of

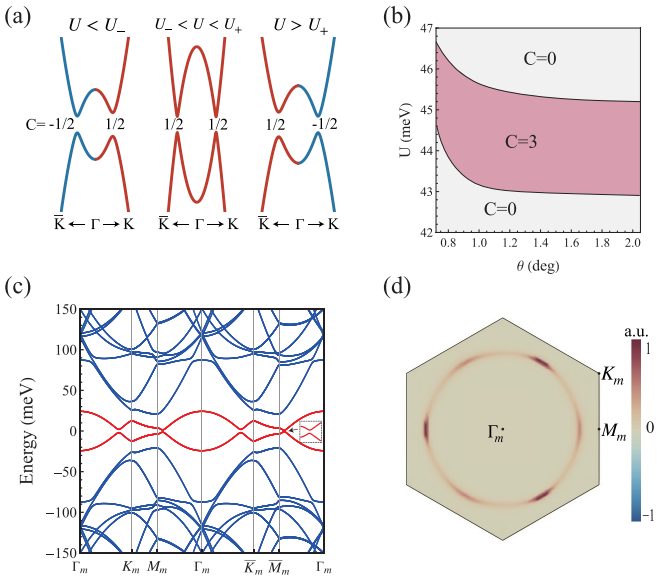

FIG. 2. (a) Band structures with increasing electric potential U for the two intertwined Dirac-cone states located along the $\overline{K}$-Γ-K path in the original untwisted case, where the two Dirac states have the same (opposite) fractional Chern number for $U_- < U < U_+$ ($U < U_-$ or $U > U_+$). (b) Typical phase diagram with the twist angle θ and the electric potential U for a twisted AFM TI thin film preserving the C_{3z} symmetry. A high-Chern-number state with $C = 3$ in the intermediate regime of U persists for the concerned twist angles. Representative band structure (c) and corresponding Berry curvature distribution (d) in the moiré BZ for the high-Chern-number ($C = 3$) state hosting two quasiflat bands near the Fermi level under a very small twist angle of 0.75°. In the above numerical calculations, the parameters are chosen typically as follows: lattice constant $a = 2$ Å, $m = 0.04$ eV, $U = 0.045$ eV, $v = 1$ eV Å, $\Delta = 0.02$ eV, $B = 60$ eV Å^2, $R_a = 200$ eV Å^3, $R_w = 200$ eV Å^3, and for simplicity only a k-independent constant coupling with a strength of $\Delta/2$ is considered in T_j's ($j = 1, 2, \ldots, 6$).

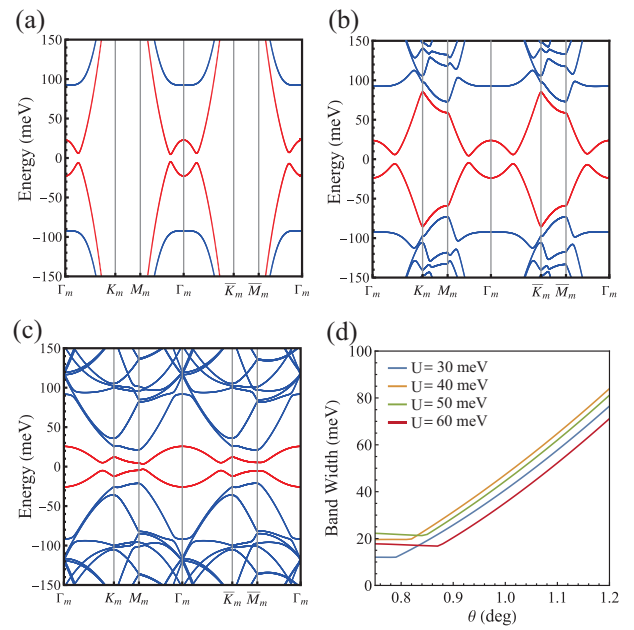

FIG. 3. Band structures in the moiré BZ of the twisted AFM TI thin film with $U = 50$ meV and gradually reduced twist angels of (a) $\theta = 2°$, (b) $\theta = 1.2°$, and (c) $\theta = 0.75°$. A significant reduction of the dispersion of the highest valence and lowest conduction bands near the Fermi level can be clearly seen, which become nearly flat in (c). (d) The evolution of the bandwidth of the highest valence band with decreasing twist angle θ. Besides θ and U, the other parameters in the numerical calculations are the same as those in Fig. 2.

which can be found in Ref. [61]. As shown in Fig. 2(a), when the potential U is smaller than U_- or larger than U_+, with $U_\pm$ given by [61]

$$U_\pm = \sqrt{v^2\Delta/B + [m \pm R_w(\Delta/B)^{3/2}]^2}, \tag{5}$$

the two intertwined Dirac-cone states (the other four Dirac-cone states are related by C_{3z} rotations) located along $\Gamma \to K$ and $\Gamma \to \overline{K}$ directions, respectively, have opposite fractional Chern numbers $\pm 1/2$. As a result, the total Chern number C equals zero at the Fermi level, whereas when $U_- < U < U_+$, the above two Dirac-cone states have identical fractional Chern numbers ($C = 1/2$), leading to a high-Chern-number state with $C = 3$.

After the twist between the top and bottom surface layers, the original band structures will get significantly modified in the moiré BZ. First, the critical electric fields $U_\pm$ where topological phase transitions happen accompanying the gap closing-and-reopening processes of the intertwined Dirac-cone states are no longer fixed and instead change with θ. A typical topological phase diagram as a function of θ and U is presented in Fig. 2(b), where both U_+ and U_- are found to increase with decreasing θ. Second, since the moiré BZ is much smaller than the original BZ, the moiré band structures are expected to have a much reduced bandwidth with less dispersive bands, as will be discussed in detail below. Most importantly, for a very small twist angle ($\theta < 1°$), a $C = 3$ high-Chern-number state hosting almost flat bands near the Fermi level can emerge. This is exemplified by the band structure of $\theta = 0.75°$ and $U = 45$ meV, shown in Fig. 2(c), where the bandwidths of the highest valence band (HVB) and the lowest conduction band (LCB) become smaller than 25 meV. We have also plotted the corresponding Berry curvature distribution in the moiré BZ in Fig. 2(d), and it can be seen that Berry curvatures are still mainly concentrated around the intertwined Dirac points located along the M_m-Γ_m-$\overline{M}_m$ directions.

IV. TWIST-ENGINEERED BAND STRUCTURES

By tuning the twist angle, the band structure of the AFM TI can be engineered in two aspects. On the one hand, the bandwidth can be reduced by decreasing θ, and the bands could become nearly flat for quite small θ. Figures 3(a)–3(c) show the evolution of a typical band structure for $U = 50$ meV with gradually decreased values of $\theta = 2°$ [Fig. 3(a)], $\theta = 1.2°$ [Fig. 3(b)], and $\theta = 0.75°$ [Fig. 3(c)], where a significant reduction of the bandwidth can be clearly seen from the particle-hole symmetric HVB and LCB. Moreover, we have explicitly plotted the bandwidth of the HVB with decreasing θ for different values of the potential, as shown in Fig. 3(d). All

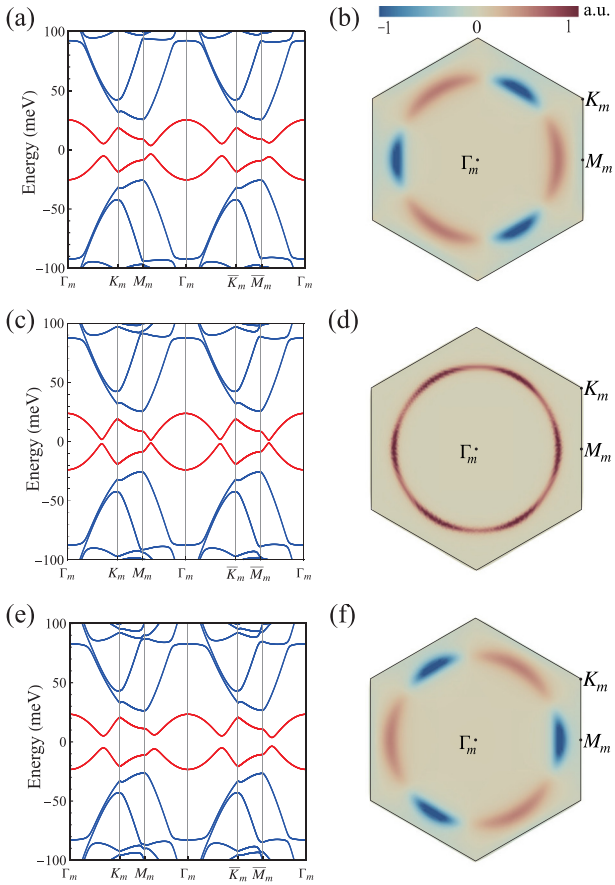

FIG. 4. Electrically tunable flat-band structures (first column) and corresponding Berry curvatures (second column) of the twisted AFM TI thin film at $\theta = 0.8^\circ$ with $U = 40$ meV ($C = 0$, first row), 45 meV ($C = 3$, second row), and 50 meV ($C = 0$, third row), respectively. The other parameters in the numerical calculations are the same as those in Fig. 2.

of them exhibit a monotonous decrease of the bandwidth with gradually reducing θ until it reaches a small critical value, beyond which the band becomes quite flat with its width around 20 meV. On the other hand, according to the phase diagram in Fig. 2(b), topological phase transitions between trivial ($C = 0$) and nontrivial ($C = 3$) could be induced by simply tuning the twist angle.

Further, we show that the topological property of the quasi-flat bands formed by the HVB and LCB near the Fermi level at small twist angles can be easily tuned by the electric field. With increasing the potential U, two successive gap closing-and-reopening processes are found to occur at U_- and U_+ from the intertwined Dirac states located along the Γ-$\overline{M}_m$ (and other two C_{3z}-symmetry related paths) and Γ-M_m directions, respectively, in the moiré BZ. As an example, we have plotted the band structures at $\theta = 0.8^\circ$ for three representative values of U, namely, $U < U_-$ [Fig. 4(a)], $U_- < U < U_+$ [Fig. 4(c)], and $U > U_+$ [Fig. 4(e)]. The corresponding Berry curvatures of the HVB are presented in Figs. 4(b), 4(d) and 4(f), respectively. The Berry curvature around the intertwined Dirac state along Γ-$\overline{M}_m$ reverses its sign from negative to positive across the transition point of U_-, as can be seen from Figs. 4(b) and 4(d). This contributes a total change of $+3$ for the Chern number of the occupied bands, thus driving a phase transition from a trivial flat-band state with $C = 0$ to a high-Chern-number ($C = 3$) nontrivial flat-band state. Similarly, the sign change of the Berry curvatures from positive to negative around the intertwined Dirac states along Γ-M_m across U_+ changes the Chern number by -3, and the flat-band system returns to the trivial $C = 0$ state.

V. SUMMARY AND DISCUSSION

In summary, based on the effective model analysis, we have proposed realizing high-Chern-number ($C = n$) flat-band states near the Fermi level in twisted AFM TI thin films preserving an n-fold rotational symmetry. The intertwined Dirac-cone states induced by anisotropic intersurface coupling are found to play a crucial role in forming these nontrivial flat bands through the twisting procedure. Furthermore, we have also demonstrated that an out-of-plane electric field could drive topological phase transitions between nontrivial ($C = n$) and trivial ($C = 0$) flat-band states. Our work not only sheds light on the significance of the recently proposed intertwined Dirac-cone states, but also open an avenue to realize high-Chern-number flat bands.

It is noteworthy that the $C = 3$ phase has already been confirmed in $MnBi_2Te_4/(Bi_2Te_3)_m/MnBi_2Te_4$ ($m = 0, 1, 2$) heterostructures through first-principles calculations [61], and thus the proposed flat-band states could hopefully be realized in these materials by moiré engineering. As for the experimental realization, the electric field (displacement field) can be applied and changed through the commonly used dual-gate technique, where both the displacement field and charge density can be simultaneously tuned [67,68]. To be more specific, the electric field potential for the typical high-Chern-number flat-band state of our work lies in the range between 40 and 50 meV, and when taking a 4-septuple-layer $MnBi_2Te_4$ thin film with a thickness of $\sim$5 nm ($\sim$1.36 nm per septuple layer) as an example, the required electric field corresponds to the displacement field between 0.08 and 0.1 V/nm (a typical dielectric constant and screening factor of $\sim$10 has been considered), which is easily accessible in experiments [67,68]. Notably, when considering lattice relaxation effects [69,70], such as an enhancement of the Fermi velocity and the change of interlayer distance with modified interlayer couplings, the corresponding critical electric field strength may get slightly changed. Nevertheless, since the Chern-insulator state corresponds to a charge neutrality single-particle gap, no correlation effects or fine-tuning fractional fillings are required, thus ensuring its stability and feasibility for observation. Interestingly, if electron-electron interactions are considered, exotic states such as a fractional Chern insulator and chiral superconductivity may emerge in these systems, which will be left for future work.

ACKNOWLEDGMENTS

This work is supported by National Key Projects for Research and Development of China (Grants No. 2021YFA1400400 and No. 2023YFA1407001), the

Fundamental Research Funds for the Central Universities (Grant No. 020414380185), the Natural Science Foundation of China (No. 92365203, No. 12104217, and No. 12074181), and the Department of Science and Technology of Jiangsu Province (BK20220032).

H.W. and Y.F. contributed equally to this work.

[1] Y. Cao, V. Fatemi, A. Demir, S. Fang, S. L. Tomarken, J. Y. Luo, J. D. Sanchez-Yamagishi, K. Watanabe, T. Taniguchi, E. Kaxiras *et al.*, Correlated insulator behaviour at half-filling in magic-angle graphene superlattices, Nature (London) **556**, 80 (2018).

[2] Y. Cao, V. Fatemi, S. Fang, K. Watanabe, T. Taniguchi, E. Kaxiras, and P. Jarillo-Herrero, Unconventional superconductivity in magic-angle graphene superlattices, Nature (London) **556**, 43 (2018).

[3] H. L. Stormer, D. C. Tsui, and A. C. Gossard, The fractional quantum Hall effect, Rev. Mod. Phys. **71**, S298 (1999).

[4] M. Levin and A. Stern, Fractional topological insulators, Phys. Rev. Lett. **103**, 196803 (2009).

[5] J. Maciejko, X.-L. Qi, A. Karch, and S.-C. Zhang, Fractional topological insulators in three dimensions, Phys. Rev. Lett. **105**, 246809 (2010).

[6] X.-L. Qi, Generic wave-function description of fractional quantum anomalous Hall states and fractional topological insulators, Phys. Rev. Lett. **107**, 126803 (2011).

[7] K. Sun, Z. Gu, H. Katsura, and S. Das Sarma, Nearly flatbands with nontrivial topology, Phys. Rev. Lett. **106**, 236803 (2011).

[8] E. Tang, J.-W. Mei, and X.-G. Wen, High-temperature fractional quantum Hall states, Phys. Rev. Lett. **106**, 236802 (2011).

[9] T. Neupert, L. Santos, C. Chamon, and C. Mudry, Fractional quantum Hall states at zero magnetic field, Phys. Rev. Lett. **106**, 236804 (2011).

[10] A. Stern, Fractional topological insulators: A pedagogical review, Annu. Rev. Condens. Matter Phys. **7**, 349 (2016).

[11] E. M. Spanton, A. A. Zibrov, H. Zhou, T. Taniguchi, K. Watanabe, M. P. Zaletel, and A. F. Young, Observation of fractional Chern insulators in a van der Waals heterostructure, Science **360**, 62 (2018).

[12] S. Yang, Z.-C. Gu, K. Sun, and S. Das Sarma, Topological flat band models with arbitrary Chern numbers, Phys. Rev. B **86**, 241112(R) (2012).

[13] A. Sterdyniak, C. Repellin, B. A. Bernevig, and N. Regnault, Series of Abelian and non-Abelian states in $C > 1$ fractional Chern insulators, Phys. Rev. B **87**, 205137 (2013).

[14] M. Barkeshli and X.-L. Qi, Topological nematic states and non-Abelian lattice dislocations, Phys. Rev. X **2**, 031013 (2012).

[15] M. Trescher and E. J. Bergholtz, Flat bands with higher Chern number in pyrochlore slabs, Phys. Rev. B **86**, 241111(R) (2012).

[16] K. Bao, H. Wang, Y. Jiang, H. Xu, and J. Wang, Isolated nearly flat higher Chern band in monolayer transition metal trihalides, arXiv:2403.07551.

[17] R. Bistritzer and A. H. MacDonald, Moiré bands in twisted double-layer graphene, Proc. Natl. Acad. Sci. USA **108**, 12233 (2011).

[18] E. Y. Andrei and A. H. MacDonald, Graphene bilayers with a twist, Nat. Mater. **19**, 1265 (2020).

[19] Y. Tang, L. Li, T. Li, Y. Xu, S. Liu, K. Barmak, K. Watanabe, T. Taniguchi, A. H. MacDonald, J. Shan *et al.*, Simulation of Hubbard model physics in WSe_2/WS_2 moiré superlattices, Nature (London) **579**, 353 (2020).

[20] E. C. Regan, D. Wang, C. Jin, M. I. Bakti Utama, B. Gao, X. Wei, S. Zhao, W. Zhao, Z. Zhang, K. Yumigeta *et al.*, Mott and generalized Wigner crystal states in WSe_2/WS_2 moiré superlattices, Nature (London) **579**, 359 (2020).

[21] Y. Shimazaki, I. Schwartz, K. Watanabe, T. Taniguchi, M. Kroner, and A. Imamoğlu, Strongly correlated electrons and hybrid excitons in a moiré heterostructure, Nature (London) **580**, 472 (2020).

[22] L. Wang, E.-M. Shih, A. Ghiotto, L. Xian, D. A. Rhodes, C. Tan, M. Claassen, D. M. Kennes, Y. Bai, B. Kim *et al.*, Correlated electronic phases in twisted bilayer transition metal dichalcogenides, Nat. Mater. **19**, 861 (2020).

[23] J. Cano, S. Fang, J. H. Pixley, and J. H. Wilson, Moiré superlattice on the surface of a topological insulator, Phys. Rev. B **103**, 155157 (2021).

[24] A. Dunbrack and J. Cano, Magic angle conditions for twisted three-dimensional topological insulators, Phys. Rev. B **106**, 075142 (2022).

[25] T. Wang, N. F. Q. Yuan, and L. Fu, Moiré surface states and enhanced superconductivity in topological insulators, Phys. Rev. X **11**, 021024 (2021).

[26] Z. Liu, H. Wang, and J. Wang, Magnetic moiré surface states and flat Chern bands in topological insulators, Phys. Rev. B **106**, 035114 (2022).

[27] G. Chaudhary, A. A. Burkov, and O. G. Heinonen, Twisted bilayers of thin film magnetic topological insulators, Phys. Rev. Res. **4**, 043034 (2022).

[28] Y. Gong, J. Guo, J. Li, K. Zhu, M. Liao, X. Liu, Q. Zhang, L. Gu, L. Tang, X. Feng, D. Zhang, W. Li, C. Song, L. Wang, P. Yu, X. Chen, Y. Wang, H. Yao, W. Duan, Y. Xu *et al.*, Experimental realization of an intrinsic magnetic topological insulator, Chin. Phys. Lett. **36**, 076801 (2019).

[29] M. M. Otrokov, I. I. Klimovskikh, H. Bentmann, D. Estyunin, A. Zeugner, Z. S. Aliev, S. Gass, A. U. B. Wolter, A. V. Koroleva, A. M. Shikin, M. Blanco-Rey, M. Hoffmann, I. P. Rusinov, A. Y. Vyazovskaya, S. V. Eremeev, Y. M. Koroteev, V. M. Kuznetsov, F. Freyse, J. Sanchez-Barriga, I. R. Amiraslanov *et al.*, Prediction and observation of an antiferromagnetic topological insulator, Nature (London) **576**, 416 (2019).

[30] D. Zhang, M. Shi, T. Zhu, D. Xing, H. Zhang, and J. Wang, Topological axion states in the magnetic insulator $MnBi_2Te_4$ with the quantized magnetoelectric effect, Phys. Rev. Lett. **122**, 206401 (2019).

[31] J. Li, Y. Li, S. Du, Z. Wang, B.-L. Gu, S.-C. Zhang, K. He, W. Duan, and Y. Xu, Intrinsic magnetic topological insulators in van der Waals layered $MnBi_2Te_4$-family materials, Sci. Adv. **5**, eaaw5685 (2019).

[32] B. Chen, F. Fei, D. Zhang, B. Zhang, W. Liu, S. Zhang, P. Wang, B. Wei, Y. Zhang, Z. Zuo *et al.*, Intrinsic magnetic topological

insulator phases in the Sb doped $MnBi_2Te_4$ bulks and thin flakes, Nat. Commun. **10**, 4469 (2019).

[33] Y. J. Chen, L. X. Xu, J. H. Li, Y. W. Li, H. Y. Wang, C. F. Zhang, H. Li, Y. Wu, A. J. Liang, C. Chen, S. W. Jung, C. Cacho, Y. H. Mao, S. Liu, M. X. Wang, Y. F. Guo, Y. Xu, Z. K. Liu, L. X. Yang, and Y. L. Chen, Topological electronic structure and its temperature evolution in antiferromagnetic topological insulator $MnBi_2Te_4$, Phys. Rev. X **9**, 041040 (2019).

[34] H. Li, S.-Y. Gao, S.-F. Duan, Y.-F. Xu, K.-J. Zhu, S.-J. Tian, J.-C. Gao, W.-H. Fan, Z.-C. Rao, J.-R. Huang, J.-J. Li, D.-Y. Yan, Z.-T. Liu, W.-L. Liu, Y.-B. Huang, Y.-L. Li, Y. Liu, G.-B. Zhang, P. Zhang, T. Kondo *et al.*, Dirac surface states in intrinsic magnetic topological insulators $EuSn_2As_2$ and $MnBi_{2n}Te_{3n+1}$, Phys. Rev. X **9**, 041039 (2019).

[35] Y.-J. Hao, P. Liu, Y. Feng, X.-M. Ma, E. F. Schwier, M. Arita, S. Kumar, C. Hu, R. Lu, M. Zeng, Y. Wang, Z. Hao, H.-Y. Sun, K. Zhang, J. Mei, N. Ni, L. Wu, K. Shimada, C. Chen, Q. Liu *et al.*, Gapless surface Dirac cone in antiferromagnetic topological insulator $MnBi_2Te_4$, Phys. Rev. X **9**, 041038 (2019).

[36] M. M. Otrokov, I. P. Rusinov, M. Blanco-Rey, M. Hoffmann, A. Y. Vyazovskaya, S. V. Eremeev, A. Ernst, P. M. Echenique, A. Arnau, and E. V. Chulkov, Unique thickness-dependent properties of the van der Waals interlayer antiferromagnet $MnBi_2Te_4$ films, Phys. Rev. Lett. **122**, 107202 (2019).

[37] H. Sun, B. Xia, Z. Chen, Y. Zhang, P. Liu, Q. Yao, H. Tang, Y. Zhao, H. Xu, and Q. Liu, Rational design principles of the quantum anomalous Hall effect in superlatticelike magnetic topological insulators, Phys. Rev. Lett. **123**, 096401 (2019).

[38] R. C. Vidal, A. Zeugner, J. I. Facio, R. Ray, M. H. Haghighi, A. U. B. Wolter, L. T. C. Bohorquez, F. Caglieris, S. Moser, T. Figgemeier *et al.*, Topological electronic structure and intrinsic magnetization in $MnBi_4Te_7$: A Bi_2Te_3 derivative with a periodic Mn sublattice, Phys. Rev. X **9**, 041065 (2019).

[39] J. Ge, Y. Liu, J. Li, H. Li, T. Luo, Y. Wu, Y. Xu, and J. Wang, High-Chern-number and high-temperature quantum Hall effect without Landau levels, Natl. Sci. Rev. **7**, 1280 (2020).

[40] C. Hu, K. N. Gordon, P. Liu, J. Liu, X. Zhou, P. Hao, D. Narayan, E. Emmanouilidou, H. Sun, Y. Liu, H. Brawer, A. P. Ramirez, L. Ding, H. Cao, Q. Liu, D. Dessau, and N. Ni, A van der Waals antiferromagnetic topological insulator with weak interlayer magnetic coupling, Nat. Commun. **11**, 97 (2020).

[41] H. Wang, D. Wang, Z. Yang, M. Shi, J. Ruan, D. Xing, J. Wang, and H. Zhang, Dynamical axion state with hidden pseudospin Chern numbers in $MnBi_2Te_4$-based heterostructures, Phys. Rev. B **101**, 081109(R) (2020).

[42] H. Fu, C.-X. Liu, and B. Yan, Exchange bias and quantum anomalous Hall effect in the $MnBi_2Te_4/CrI_3$ heterostructure, Sci. Adv. **6**, eaaz0948 (2020).

[43] B. Lian, Z. Liu, Y. Zhang, and J. Wang, Flat Chern band from twisted bilayer $MnBi_2Te_4$, Phys. Rev. Lett. **124**, 126402 (2020).

[44] P. M. Sass, J. Kim, D. Vanderbilt, J. Yan, and W. Wu, Robust *A*-type order and spin-flop transition on the surface of the antiferromagnetic topological insulator $MnBi_2Te_4$, Phys. Rev. Lett. **125**, 037201 (2020).

[45] C. Liu, Y. Wang, H. Li, Y. Wu, Y. Li, J. Li, K. He, Y. Xu, J. Zhang, and Y. Wang, Robust axion insulator and Chern insulator phases in a two-dimensional antiferromagnetic topological insulator, Nat. Mater. **19**, 522 (2020).

[46] M. Gu, J. Li, H. Sun, Y. Zhao, C. Liu, J. Liu, H. Lu, and Q. Liu, Spectral signatures of the surface anomalous Hall effect in magnetic axion insulators, Nat. Commun. **12**, 3524 (2021).

[47] H. Li, C.-Z. Chen, H. Jiang, and X. C. Xie, Coexistence of quantum Hall and quantum anomalous Hall phases in disordered $MnBi_2Te_4$, Phys. Rev. Lett. **127**, 236402 (2021).

[48] A. Gao, Y.-F. Liu, C. Hu, J.-X. Qiu, C. Tzschaschel, B. Ghosh, S.-C. Ho, D. Bérubé, R. Chen, H. Sun *et al.*, Layer Hall effect in a 2D topological axion antiferromagnet, Nature (London) **595**, 521 (2021).

[49] C. Liu, Y. Wang, M. Yang, J. Mao, H. Li, Y. Li, J. Li, H. Zhu, J. Wang, L. Li *et al.*, Magnetic-field-induced robust zero Hall plateau state in $MnBi_2Te_4$ Chern insulator, Nat. Commun. **12**, 4647 (2021).

[50] T. Zhu, H. Wang, and H. Zhang, Floquet engineering of magnetic topological insulator $MnBi_2Te_4$ films, Phys. Rev. B **107**, 085151 (2023).

[51] Y. Bai, Y. Li, J. Luan, R. Liu, W. Song, Y. Chen, P.-F. Ji, Q. Zhang, F. Meng, B. Tong, L. Li, Y. Jiang, Z. Gao, L. Gu, J. Zhang, Y. Wang, Q.-K. Xue, K. He, Y. Feng, and X. Feng, Quantized anomalous Hall resistivity achieved in molecular beam epitaxy-grown $MnBi_2Te_4$ thin films, Nat. Sci. Rev. **11**, nwad189 (2023).

[52] N. Wang, D. Kaplan, Z. Zhang, T. Holder, N. Cao, A. Wang, X. Zhou, F. Zhou, Z. Jiang, C. Zhang, S. Ru, H. Cai, K. Watanabe, T. Taniguchi, B. Yan, and W. Gao, Quantum-metric-induced nonlinear transport in a topological antiferromagnet, Nature (London) **621**, 487 (2023).

[53] A. Gao, Y.-F. Liu, J.-X. Qiu, B. Ghosh, T. V. Trevisan, Y. Onishi, C. Hu, T. Qian, H.-J. Tien, S.-W. Chen, M. Huang, D. Bérubé, H. Li, C. Tzschaschel, T. Dinh, Z. Sun, S.-C. Ho, S.-W. Lien, B. Singh, K. Watanabe *et al.*, Quantum metric nonlinear Hall effect in a topological antiferromagnetic heterostructure, Science **381**, 181 (2023).

[54] N. H. Jo, L.-L. Wang, R.-J. Slager, J. Yan, Y. Wu, K. Lee, B. Schrunk, A. Vishwanath, and A. Kaminski, Intrinsic axion insulating behavior in antiferromagnetic $MnBi_6Te_{10}$, Phys. Rev. B **102**, 045130 (2020).

[55] J.-Y. You, X.-J. Dong, B. Gu, and G. Su, Electric field induced topological phase transition and large enhancements of spin-orbit coupling and Curie temperature in two-dimensional ferromagnetic semiconductors, Phys. Rev. B **103**, 104403 (2021).

[56] S. Du, P. Tang, J. Li, Z. Lin, Y. Xu, W. Duan, and A. Rubio, Berry curvature engineering by gating two-dimensional antiferromagnets, Phys. Rev. Res. **2**, 022025(R) (2020).

[57] W.-Y. Shan, H.-Z. Lu, and S.-Q. Shen, Effective continuous model for surface states and thin films of three-dimensional topological insulators, New J. Phys. **12**, 043048 (2010).

[58] H.-Z. Lu, W.-Y. Shan, W. Yao, Q. Niu, and S.-Q. Shen, Massive Dirac fermions and spin physics in an ultrathin film of topological insulator, Phys. Rev. B **81**, 115407 (2010).

[59] D. Wang, H. Wang, and H. Zhang, Dirac fermion approach and its application to design high Chern numbers in magnetic topological insulator multilayers, Phys. Rev. B **107**, 155114 (2023).

[60] D. Wang, H. Wang, D. Xing, and H. Zhang, Three-Dirac-fermion approach to unexpected universal gapless surface states in van der Waals magnetic topological insulators, Sci. China: Phys. Mech. Astron. **66**, 297211 (2023).

[61] Y. Fan, H. Wang, P. Tang, S. Murakami, X. Wan, H. Zhang, and D. Xing, Symmetry-driven anisotropic coupling effect in antiferromagnetic topological insulator: Mechanism for a quantum anomalous Hall state with a high Chern number, Phys. Rev. B **110**, 035139 (2024).

[62] L. Fu, Hexagonal warping effects in the surface states of the topological insulator Bi_2Te_3, Phys. Rev. Lett. **103**, 266801 (2009).

[63] G. Naselli, A. G. Moghaddam, S. Di Napoli, V. Vildosola, I. C. Fulga, J. van den Brink, and J. I. Facio, Magnetic warping in topological insulators, Phys. Rev. Res. **4**, 033198 (2022).

[64] H.-P. Sun, C. M. Wang, S.-B. Zhang, R. Chen, Y. Zhao, C. Liu, Q. Liu, C. Chen, H.-Z. Lu, and X. C. Xie, Analytical solution for the surface states of the antiferromagnetic topological insulator $MnBi_2Te_4$, Phys. Rev. B **102**, 241406(R) (2020).

[65] C. Lei, S. Chen, and A. H. MacDonald, Magnetized topological insulator multilayers, Proc. Natl. Acad. Sci. USA **117**, 27224 (2020).

[66] C.-X. Liu, X.-L. Qi, H. J. Zhang, X. Dai, Z. Fang, and S.-C. Zhang, Model Hamiltonian for topological insulators, Phys. Rev. B **82**, 045122 (2010).

[67] G. Chen, A. L. Sharpe, E. J. Fox, Y.-H. Zhang, S. Wang, L. Jiang, B. Lyu, H. Li, K. Watanabe, T. Taniguchi *et al.*, Tunable correlated Chern insulator and ferromagnetism in a moiré superlattice, Nature (London) **579**, 56 (2020).

[68] Y. Cao, D. Rodan-Legrain, O. Rubies-Bigorda, J. M. Park, K. Watanabe, T. Taniguchi, and P. Jarillo-Herrero, Tunable correlated states and spin-polarized phases in twisted bilayer–bilayer graphene, Nature (London) **583**, 215 (2020).

[69] N. N. T. Nam and M. Koshino, Lattice relaxation and energy band modulation in twisted bilayer graphene, Phys. Rev. B **96**, 075311 (2017).

[70] N. Leconte, S. Javvaji, J. An, A. Samudrala, and J. Jung, Relaxation effects in twisted bilayer graphene: A multiscale approach, Phys. Rev. B **106**, 115410 (2022).